LETTERS

Single-mode heat conduction by photons

Matthias Meschke[1], Wiebke Guichard[1,2] & Jukka P. Pekola[1]

The thermal conductance of a single channel is limited by its unique quantum value G_Q, as was shown theoretically[1] in 1983. This result closely resembles the well-known quantization of electrical conductance in ballistic one-dimensional conductors[2,3]. Interestingly, all particles—irrespective of whether they are bosons or fermions—have the same quantized thermal conductance[4,5] when they are confined within dimensions that are small compared to their characteristic wavelength. The single-mode heat conductance is particularly relevant in nanostructures. Quantized heat transport through submicrometre dielectric wires by phonons has been observed[6], and it has been predicted to influence cooling of electrons in metals at very low temperatures due to electromagnetic radiation[7]. Here we report experimental results showing that at low temperatures heat is transferred by photon radiation, when electron–phonon[8] as well as normal electronic heat conduction is frozen out. We study heat exchange between two small pieces of normal metal, connected to each other only via superconducting leads, which are ideal insulators against conventional thermal conduction. Each superconducting lead is interrupted by a switch of electromagnetic (photon) radiation in the form of a DC-SQUID (a superconducting loop with two Josephson tunnel junctions). We find that the thermal conductance between the two metal islands mediated by photons indeed approaches the expected quantum limit of G_Q at low temperatures. Our observation has practical implications—for example, for the performance and design of ultra-sensitive bolometers (detectors of far-infrared light) and electronic micro-refrigerators[9], whose operation is largely dependent on weak thermal coupling between the device and its environment.

To get a picture of the radiative thermal coupling, we start by considering two resistors at temperatures T_{e1} and T_{e2}, whose resistances are R_1 and R_2, respectively, connected via a frequency $(\omega/2\pi)$ dependent impedance $Z(\omega)$; see Fig. 1. For simplicity we assume $Z(\omega)$ to be fully reactive, so that only the two resistors emit and absorb noise heating. The net power flow P_v between the two resistors from 1 to 2 due to the electron–photon coupling is then given by[1,7]:

$$P_v = \int_0^\infty \frac{d\omega}{2\pi} \frac{4R_1R_2}{|Z_t(\omega)|^2} \hbar\omega[n_1(\omega) - n_2(\omega)] \quad (1)$$

Here, $Z_t(\omega) \equiv R_1 + R_2 + Z(\omega)$ is the total series impedance of the circuit, and $n_i(\omega) \equiv [\exp(\hbar\omega/k_B T_{ei}) - 1]^{-1}$ are the boson occupation factors at the temperatures of the resistors $i = 1, 2$. Specifically, for a lossless direct connection of the two resistors, $Z(\omega) \equiv 0$, we can integrate equation (1) with the result:

$$P_v^{Z=0} = r_0 \frac{\pi k_B^2}{12\hbar}\left(T_{e1}^2 - T_{e2}^2\right) \quad (2)$$

Here $r_0 \equiv 4R_1R_2/(R_1 + R_2)^2$ is the matching factor, which obtains its maximum value of unity when $R_1 = R_2$. Thermal conductance by the photonic coupling, G_v (defined as the linear response of P_v for small temperature difference $\Delta T \equiv T_{e1} - T_{e2}$ around $T \equiv (T_{e1} + T_{e2})/2$), can then be obtained from equation (2) for the lossless connection as

$$G_v = r_0 G_Q \quad (3)$$

where $G_Q = \frac{\pi k_B^2}{6\hbar} T$ is the quantum of thermal conductance. Thus G_v attains the maximum value for a single transmission channel, G_Q, in a matched circuit. This result is predicted to hold not only for such photon-mediated coupling, but much more generally for carriers of arbitrary exclusion statistics[10,11] from bosons to fermions[4,5,12–14]. Note that discussion on massless bosons such as photons or phonons is identical in detail[1], with proper definition of channel transmission in each case. Quantized thermal conductance was observed for the first time in phonons in ref. 6.

Owing to its relatively weak temperature dependence, $\propto T$, electron–photon coupling is expected to become the dominant relaxation means at sufficiently low T. The competing electron–phonon thermal conductance G_{ep} behaves normally as $G_{ep} \approx 5\Sigma\Omega T^4$, where Σ is a material parameter and Ω is the volume of the resistor. This result derives from the expression for heat flux from electrons to lattice, $P_{ep} \approx \Sigma\Omega(T_{ei}^5 - T_0^5)$, where T_{ei} and T_0 are the temperatures of the electrons in the resistor and of the lattice, respectively[8]. Equating G_v from equation (3) and G_{ep}, one finds the cross-over temperature, T_{cr}, below which the photonic conductance should

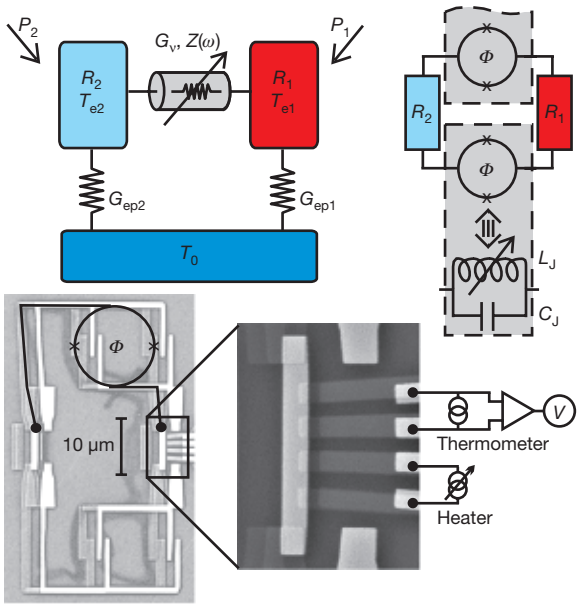

Figure 1 | The system under investigation. At the top, we show thermal (left) and electrical (right) models; at the bottom, a scanning electron micrograph of the device (left), and a magnified view of resistor 1 with four adjoining NIS and two NS contacts (right). See text for details.

[1]Low Temperature Laboratory, Helsinki University of Technology, PO Box 3500, 02015 TKK, Finland. [2]Université Joseph Fourier and LCMI-CNRS, BP 166, 25 Avenue des Martyrs, 38042 Grenoble cedex 9, France.

dominate[7]: $T_{cr} = [r_0 \pi k_B{}^2/(30\hbar\Sigma\Omega)]^{1/3}$. For typical metals, for which $\Sigma \approx 10^9\,W\,m^{-3}\,K^{-5}$, for mesoscopic resistors with $\Omega \approx 10^{-20}\,m^3$, and for matching where r_0 is not too low as compared to unity, one obtains $T_{cr} \approx 100$–200 mK. Such temperatures are in the range of experiments that we describe here. By state-of-the-art electron-beam lithography one can obtain metallic islands of volumes as small as $<10^{-24}\,m^3$ (ref. 15), and there T_{cr} could be as high as several kelvin.

To investigate the electron–photon thermal conduction experimentally, we have embedded a tunable impedance between the two resistors. This allows us to measure the modulation of P_v, or G_v, in response to the externally controllable impedance $Z(\omega)$. In practice the two resistors are connected to each other symmetrically by two aluminium superconducting lines, interrupted by a DC-SQUID (superconducting quantum interference device) in each line, as shown in the electron micrograph and in the electrical model in Fig. 1. These SQUIDs serve as the thermal switches between the resistors, as will be described below.

The structures have been fabricated by electron-beam lithography and three angle shadow evaporation. The film thickness of the superconducting lines is 20 nm. The two AuPd resistors are nominally identical—6.6 μm long, 0.8 μm wide and 15 nm thick. Their resistances are $R_i \approx 200\,\Omega$ each. One of them, say R_1, is connected by four NIS (normal–insulator–superconductor) tunnel junctions to external aluminium leads to allow for thermometry[16] and Joule heating. The normal state resistance of each NIS junction is about 50 kΩ. The resistors are connected by direct NS contacts to the superconducting lines in between, without a tunnel barrier. They are, however, long enough such that they are not noticeably affected by proximity superconductivity. This is verified by the measured tunnel characteristics of the nearby NIS tunnel junctions. Owing to the superconductors being at a low working temperature, which is typically a factor of ten below the critical temperature $T_C \approx 1.2$ K of aluminium, the normal electronic thermal conductance along the lines is efficiently suppressed.

Each DC-SQUID can be modelled as a parallel connection of a Josephson inductance L_J and capacitance C_J. $L_J \approx \hbar/(2eI_C)$ can be tuned by external magnetic flux Φ threading through the DC-SQUID loop, as the critical current is $I_C \approx I_{C0}\,|\cos(\pi\Phi/\Phi_0)|$. Here I_{C0} is the Ambegaokar-Baratoff critical current[17] determined by geometry and materials, and $\Phi_0 = h/2e \approx 2\times10^{-15}$ Wb is the flux quantum. Capacitance C_J is a constant determined by geometry and materials.

The length of the lines connecting resistors R_1 and R_2 is ~30 μm, that is, much shorter than the typical thermal wavelength $\lambda_{th} = 2\pi\hbar c/(k_B T)$, which is several centimetres at 100 mK; here $c \approx 10^8\,m\,s^{-1}$ is the speed of light on a silicon substrate. Therefore we do not need to consider a distributed electrical model with a transmission line, but instead $Z(\omega)$ is effectively a lumped series connection of two LC circuits, that is, $Z(\omega) = i2\omega L_J/[1-(\omega/\omega_0)^2]$. Here $\omega_0 = (L_J C_J)^{-1/2}$, and we have assumed for simplicity that the two DC-SQUIDs are identical and that they are exposed to the same magnetic field. This is expected to be a good approximation in view of the symmetric experimental configuration. The net heat flow between 1 and 2 is then given by

$$P_v = \frac{\pi k_B^2}{12\hbar}\left(r_1 T_{e1}^2 - r_2 T_{e2}^2\right) \qquad (4)$$

where the matching parameters r_i now depend on temperature as:

$$r_i = \frac{6r_0}{\pi^2}\int_0^\infty dx \frac{x}{e^x-1}\left[1+\frac{(\omega_{th,i}\tau_R)^2 x^2}{\left[1-(\omega_{th,i}/\omega_0)^2 x^2\right]^2}\right]^{-1} \qquad (5)$$

Above we have defined $\omega_{th,i} \equiv k_B T_{ei}/\hbar$ and $\tau_R \equiv L_J/[(R_1+R_2)/2]$.

For the full description, we still need a thermal model incorporating the two competing relaxation mechanisms, due to photons and phonons, respectively. This is schematically depicted in Fig. 1, where the temperature in each resistor tends to relax via electron–phonon coupling $G_{ep,i}$ to the constant temperature T_0 of the bath, and towards a common temperature of the two resistors via the tunable photonic conductance G_v. P_i denotes the external heat leak into resistor i: owing to wire connections, P_1 has a significant non-zero value even in the absence of intentional heating, whereas P_2 turns out to be very small, as the corresponding resistor is not connected directly to external leads. We may describe the steady state of the system by power balance equations:

$$P_i = \pm\frac{\pi k_B^2}{12\hbar}\left(r_1 T_{e1}^2 - r_2 T_{e2}^2\right) + \Sigma\Omega_i\left(T_{ei}^5 - T_0^5\right),\ i=1,2 \qquad (6)$$

where ± equals + for $i = 1$, and − for $i = 2$, and Ω_i is the volume of resistor i. Equation (6) combined with equation (5) can be solved numerically to obtain the temperatures T_{ei} under given conditions. We note that the thermal analysis of the system would be even simpler, if resistor 2 were very large in size (but still with the same resistance) to fix T_{e2} at T_0. Yet such a design would introduce complications in fabrication, and also the simple lumped element electrical analysis would eventually fail.

The experiments were performed in a ^{3}He-^{4}He dilution refrigerator at temperatures from 30 mK up to several hundred mK. All the measurement wiring was carefully filtered and essentially only DC signals were used. One of the NIS tunnel junction pairs connected to resistor 1 was used as a thermometer by applying a small (2.4 pA) DC current I_P through it and by measuring the corresponding temperature dependent voltage V_P. When biased at a low enough current, high sensitivity is obtained without excessive self-heating or self-cooling effects[9]. The NIS thermometer is then calibrated by measuring V_P against the bath temperature T_0, by slowly sweeping the temperature of the mixing chamber through the range of interest, from about 40 mK up to about 500 mK. Figure 2a shows such a calibration run. The dependence of $R \equiv V_P/I_P$ on temperature turns out to be linear in the range 100–300 mK, which is as expected at

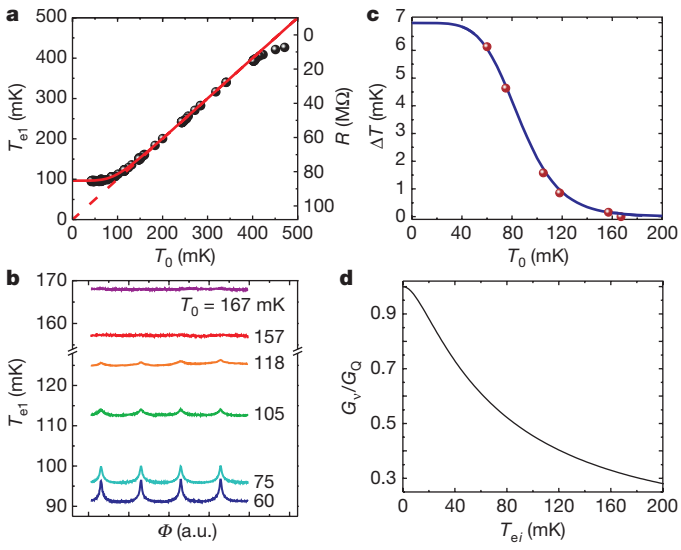

Figure 2 | Results of the measurements in the absence of extra heating. **a**, The NIS thermometer calibration. The dots indicate the measured resistance (right scale) at the bias current of 2.4 pA as a function of bath temperature T_0. The lines show calculated T_{e1} (left scale) versus T_0 for $P_1 = 1$ fW (solid line) and for $P_1 = 0$ (dashed line). **b**, Flux modulation of T_{e1} recorded at the values of T_0 indicated. **c**, The measured amplitude (symbols) of temperature modulation plotted against T_0 and compared to the theoretical model (line) as described in the text, assuming $P_1 = 1$ fW according to **a**. **d**, The ratio of the photonic thermal conductance G_v in our circuit at $\Phi = 0$ and the quantum of thermal conductance G_Q as a function of the electron temperature T_{ei}. This plot is a calculated result based on the experimentally determined values of the system parameters, as given in the text.

temperatures well below T_C (refs 9, 16). At low temperatures, R saturates, which we ascribe predominantly to residual heat input into resistor 1 owing to coupling to the environment and to self-heating. By setting $P_1 = 1$ fW, we obtain the measured R versus T_0 curve through equation (6) at half-integer values of Φ/Φ_0, where the photonic contribution can be neglected. We use this value of P_1 in analysing the actual measurements.

The measurements of thermal coupling are then done by stabilizing the bath at a desired temperature. Then we apply slow sweeps ($\sim 1\Phi_0\,\mathrm{min}^{-1}$) of external magnetic flux, which threads the two DC-SQUID loops nominally identically. A typical amplitude of the field sweep is such that it corresponds to 4–5 flux quanta through each DC-SQUID. In our geometry, this corresponds to a field of about 100 μT. The NIS thermometer reading is then averaged over several tens of such field sweeps, to measure accurately the periodic variation of T_{e1} in response to the field sweep.

Figure 2b shows results of a measurement at a few bath temperatures as described above. We see that the modulation of T_{e1} in response to magnetic flux Φ is about 6 mK at the lowest bath temperature and it decreases monotonically when T_0 is increased. Based on this data and our electrical and thermal models above, we expect that the maxima in T_{e1} correspond to the weakest electron–photon coupling at half-integer values of Φ/Φ_0. In Fig. 2c we plot with circles the corresponding modulation amplitude of T_{e1} between its maximum and minimum values, $\Delta T \equiv T_{e1,max} - T_{e1,min}$, as a function of T_0 for the experimental data in Fig. 2b. We have added to the figure a solid line from our theoretical model, assuming $R_1 = R_2$, $P_1 = 1$ fW, $P_2 = 0$ and $I_{C0} = 20$ nA. The last value is a fit parameter, as we cannot measure it directly in our geometry, but it is in line with the measured values of critical currents of DC-SQUIDs that we fabricated with the same parameters separately. We set $C_J = 15$ fF, based on the geometry of the device. Additionally, we use a typical value $\Sigma = 2 \times 10^9\,\mathrm{W\,K^{-5}\,m^{-3}}$ (ref. 8), and $\Omega_i = 6 \times 10^{-20}\,\mathrm{m^3}$ for both resistors. The latter corresponds to the volume of each resistor excluding the overlap areas of NS contacts. The agreement between the experiment and the model is very good, and we therefore use these very realistic parameters in analysing all the results reported here. These data imply (Fig. 2d) that r_i at integer values of Φ/Φ_0 lies in the range 0.6–0.3, when we vary temperature from ~60 mK (the approximate value of T_{e2} at the minimum bath temperature) up to 200 mK, that is, the electron–photon conductance is about one-half of its quantum value in our experiment. Note that G_v is expected to approach the quantum of thermal conductance upon lowering temperature, as the thermal frequency $\omega_{th,i}$ decreases linearly with T_e, and the line impedance at low frequencies, determined by L_J, decreases likewise.

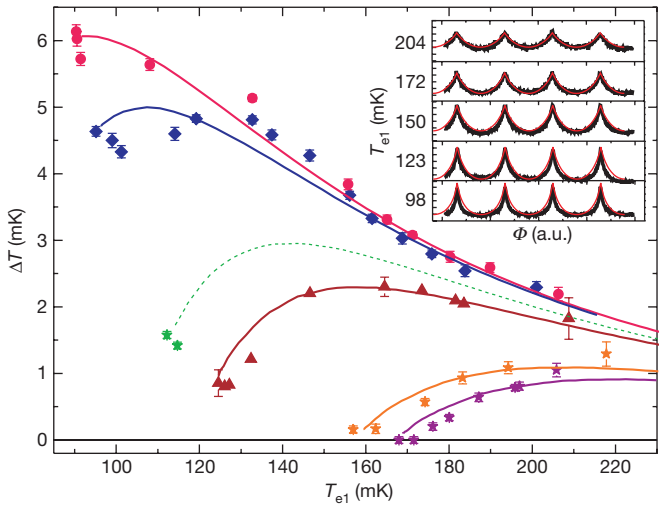

Figure 3 | Results of the measurement of ΔT with variable amounts of Joule heating applied to resistor 1. ΔT is the modulation of T_{e1} when flux is varied; Joule heating was in the range 0–60 fW. Different sets of data and lines correspond to different bath temperatures T_0. From top to bottom, $T_0 = 60$ mK, 75 mK, 105 mK, 118 mK, 157 mK and 167 mK. The symbols refer to experimental data, and lines are from the theoretical model described. The error bars display the standard deviation between the measured thermometer reading (versus Φ) and the empirical fit function to it. Inset, primary data in form of T_{e1} against flux, under different input power levels and at $T_0 = 75$ mK. Black lines are from the experiment and red ones from the theory. The full temperature range in each panel is 6 mK.

Next we present experiments where external power was applied to resistor 1, using the second pair of tunnel junctions connected to it as a heater. Figure 3 demonstrates such measurements at different bath temperatures. Compared to the data at the lowest bath temperature of 60 mK, where an essentially monotonic decrease of ΔT can be observed, the intermediate bath temperature data demonstrates a non-monotonic dependence: there is an initial increase of the signal on increasing the heating, and then slow decrease towards higher power levels and higher T_{e1}. Finally, at the highest values of T_0, the signal is first absent but emerges upon increasing the input power. This behaviour arises because by applying Joule heating to just one resistor, we can establish a larger temperature difference between the two. Yet at large enough levels of P_1, the overall temperature of the system increases, and the significance of the photon coupling with respect to electron–phonon coupling is diminishing, and the temperature modulation becomes very weak. All these dependences are fully consistent with our theoretical modelling of the system, and we obtain quantitative agreement with the data by using the same electrical and thermal parameters of the system as when modelling data of Fig. 2. The theoretical lines in Fig. 3 are the result of this modelling. In the inset of Fig. 3 we show a few full modulation curves of T_{e1} versus Φ at a bath temperature of 75 mK. The black lines are from experiment and the red ones from the theoretical model. The theoretical lines capture the main features of the shape of the experimental curves.

Our experiment demonstrates what was proposed recently[7]: it is not justified to assume that an electron system like the one discussed here would be efficiently decoupled from the environment once the electron–phonon coupling is suppressed at low temperatures. The observed $\propto T$ photonic conductance thus has implications for the performance and design of micro-bolometers and calorimeters, where efficient suppression of thermal coupling is usually taken for granted. Owing to better coupling to the environment by photon conductance, the expected sensitivity of such devices is reduced, and their noise is enhanced. On the other hand, this mechanism could possibly provide a way to tune the thermal coupling of a bolometer to the heat bath in order to optimize its operation, which is a trade-off between sensitivity and bandwidth. The radiation of heat could also help to remove excessive heat—for example, from dissipative shunt resistors of ultra-sensitive or very low temperature SQUIDs[18], or at the back side of an electronic micro-refrigerator[19]. Furthermore, the photonic coupling could act as a mediator of decoherence: for example, in solid-state quantum coherent devices[20]. The strength of this harmful effect depends (as in our present experiment) critically on the matching between the noise source and the system that it affects.

Received 16 May; accepted 21 September 2006.

1. Pendry, J. B. Quantum limits to flow of information and entropy. *J. Phys. A* **16**, 2161–2171 (1983).
2. van Wees, B. J. *et al.* Quantized conductance of point contacts in a two-dimensional electron-gas. *Phys. Rev. Lett.* **60**, 848–850 (1988).
3. Wharam, D. A. *et al.* One-dimensional transport and the quantisation of the ballistic resistance. *J. Phys. C* **21**, L209–L214 (1988).
4. Rego, L. G. C. & Kirczenow, G. Fractional exclusion statistics and the universal quantum of thermal conductance: A unifying approach. *Phys. Rev. B* **59**, 13080–13086 (1999).
5. Blencowe, M. P. & Vitelli, V. Universal quantum limits on single-channel information, entropy, and heat flow. *Phys. Rev. B* **62**, 052104 (2000).

6. Schwab, K., Henriksen, E. A., Worlock, J. M. & Roukes, M. L. Measurement of the quantum of thermal conductance. *Nature* **404,** 974–977 (2000).
7. Schmidt, D. R., Schoelkopf, R. J. & Cleland, A. N. Photon-mediated thermal relaxation of electrons in nanostructures. *Phys. Rev. Lett.* **93,** 045901 (2004).
8. Roukes, M. L., Freeman, M. R., Germain, R. S., Richardson, R. C. & Ketchen, M. B. Hot electrons and energy transport in metals at millikelvin temperatures. *Phys. Rev. Lett.* **55,** 422–425 (1985).
9. Giazotto, F., Heikkilä, T. T., Luukanen, A., Savin, A. M. & Pekola, J. P. Opportunities for mesoscopics in thermometry and refrigeration: Physics and applications. *Rev. Mod. Phys.* **78,** 217–274 (2006).
10. Wilczek, F. Quantum mechanics of fractional-spin particles. *Phys. Rev. Lett.* **49,** 957–959 (1982).
11. Haldane, F. D. M. ''Fractional statistics'' in arbitrary dimensions: A generalization of the Pauli principle. *Phys. Rev. Lett.* **67,** 937–940 (1991).
12. Kane, C. L. & Fisher, M. P. A. Thermal transport in a Luttinger liquid. *Phys. Rev. Lett.* **76,** 3192–3195 (1996).
13. Kane, C. L. & Fisher, M. P. A. Quantized thermal transport in the fractional quantum Hall effect. *Phys. Rev. B* **55,** 15832–15837 (1997).
14. Greiner, A., Reggiani, L., Kuhn, T. & Varani, L. Thermal conductivity and Lorenz number for one-dimensional ballistic transport. *Phys. Rev. Lett.* **78,** 1114–1117 (1997).
15. Pashkin, Yu A., Nakamura, Y. & Tsai, J. S. Room-temperature Al single-electron transistor made by electron-beam lithography. *Appl. Phys. Lett.* **76,** 2256–2258 (2000).
16. Nahum, M. & Martinis, J. M. Ultrasensitive-hot-electron microbolometer. *Appl. Phys. Lett.* **63,** 3075–3077 (1993).
17. Ambegaokar, V. & Baratoff, A. Tunneling between superconductors. *Phys. Rev. Lett.* **10,** 486–489 (1963).
18. Savin, A. M., Pekola, J. P., Averin, D. V. & Semenov, V. K. Thermal budget of superconducting digital circuits at subkelvin temperatures. *J. Appl. Phys.* **99,** 084501 (2006).
19. Clark, A. M., Williams, A., Ruggiero, S. T., van den Berg, M. L. & Ullom, J. N. Practical electron-tunneling refrigerator. *Appl. Phys. Lett.* **84,** 625–627 (2004).
20. Makhlin, Yu, Schön, G. & Shnirman, A. Quantum-state engineering with Josephson-junction devices. *Rev. Mod. Phys.* **73,** 357–400 (2001).

Acknowledgements We thank M. Paalanen, D. Averin, A. Luukanen, H. Pothier, F. Hekking and G. Schön for comments, and the Academy of Finland (TULE) and the EC-funded ULTI project for financial support.

Author Information Reprints and permissions information is available at www.nature.com/reprints. The authors declare no competing financial interests. Correspondence and requests for materials should be addressed to J.P.P. (jukka.pekola@tkk.fi).